RSC Advances

PAPER

View Article Online
View Journal | View Issue

Cite this: *RSC Adv.*, 2017, **7**, 33408

Edge-controlled half-metallic ferromagnetism and direct-gap semiconductivity in ZrS_2 nanoribbons

H. Y. Lv,[a] W. J. Lu,*[a] J. Y. Li,[a] R. C. Xiao,[a] M. J. Wei,[a] P. Tong,[a] X. B. Zhu[a] and Y. P. Sun*[abc]

Received 12th May 2017
Accepted 20th June 2017

DOI: 10.1039/c7ra05362b

rsc.li/rsc-advances

The electronic and magnetic properties of ZrS_2 nanoribbons (NRs) are investigated based on first principles calculations. It is found that the ZrS_2 NRs with armchair edges are all indirect band gap semiconductors without magnetism, and the band gap exhibits odd–even oscillation behavior with the increase of the ribbon width. For the NRs with zigzag edges, those with both edges S-terminated are nonmagnetic direct band gap semiconductors, and the gap decreases monotonically as a function of the ribbon width. However, the NRs with one edge S-terminated and the other edge Zr-terminated are ferromagnetic half-metals, while those with both edges Zr-terminated tend to be ferromagnetic half-metals when the width $N \geq 9$. The magnetism of both systems mainly originates from the unsaturated edge Zr atoms. Depending on the different edge configurations and ribbon widths, the ZrS_2 NRs exhibit versatile electronic and magnetic properties, making them promising candidates for applications in electronics and spintronics.

1 Introduction

The electronic and magnetic properties of nanoscale materials have been the subject of extensive research due to their potential applications in electronics and spintronics. Carbon-based systems, graphene for example, are among the most studied low-dimensional materials. Graphene has a high mobility at room temperature, making it a promising candidate for future information technology. However, the lack of an intrinsic band gap has limited its practical applications. Cutting two-dimensional (2D) graphene into one-dimensional (1D) nanoribbons (NRs) can open the band gap in graphene, which was first predicted theoretically[1] and then verified by experiments.[2] Because of the additional edge states unique to the dimensionality, 1D NRs could exhibit rich properties which can be further tuned by modifying their edges. It was found that the narrow zigzag graphene NR is semiconducting with the two edges antiferromagnetically coupled to each other.[1] In addition, the graphene NR can be converted into a half-metal in different ways, such as by applying a homogeneous electrical field[3] or by chemical decoration at the edges.[4,5]

Besides graphene, low-dimensional transition metal dichalcogenides, TMDs (with the formula MX_2, where M = transition metal and X = S, Se or Te), are another important material that has received considerable attention. Different from graphene, single layer MX_2 has three atomic layers, with an M-layer sandwiched between two X-layers. As a typical representative of TMDs, single layer MoS_2 is a direct band gap semiconductor.[6,7] An intrinsic 2D MoS_2 monolayer is nonmagnetic. However, distinct electronic and magnetic properties were reported for 1D MoS_2 NRs, that is, armchair MoS_2 NRs are nonmagnetic semiconductors, while zigzag MoS_2 NRs have ferromagnetic (FM) and metallic ground states.[8,9] WS_2 NRs exhibit similar properties to MoS_2 NRs.[10] The zigzag edge-related ferromagnetism was then observed experimentally in MoS_2 (ref. 11–14) and WS_2 (ref. 14 and 15) nanosheets. Furthermore, the electronic and magnetic properties of MoS_2 NRs can be modified by edge passivation[16] or by applying an external strain and/or electric field.[17–20] It was theoretically predicted that by applying a transverse electrical field, the insulator–metal transition occurs and ferromagnetism emerges beyond a critical electric field in the armchair MoS_2 NRs.[19]

Both MoS_2 and WS_2 crystallize in the honeycomb (H) structure. ZrS_2 is another kind of TMD, which crystallizes in the centered honeycomb (T) structure. Different from the MoS_2 monolayer, single layer ZrS_2 is an indirect band gap semiconductor.[21] In experiments, 1D ZrS_2 NRs have been synthesized by the process of chemical vapor transport and vacuum pyrolysis.[22,23] But what different properties do the 1D NRs present? In the present work, we investigate the electronic and magnetic properties of a series of ZrS_2 NRs. The results show that depending on the different edge configurations, the ZrS_2 NRs can be indirect band gap semiconductors, direct band gap

[a]*Key Laboratory of Materials Physics, Institute of Solid State Physics, Chinese Academy of Sciences, Hefei 230031, People's Republic of China. E-mail: wjlu@issp.ac.cn; ypsun@issp.ac.cn; Fax: +86-551-65591434; Tel: +86-551-65591439*

[b]*High Magnetic Field Laboratory, Chinese Academy of Sciences, Hefei 230031, People's Republic of China*

[c]*Collaborative Innovation Center of Advanced Microstructures, Nanjing University, Nanjing, 210093, People's Republic of China*

semiconductors, antiferromagnetic (AFM) metals or FM half-metals, exhibiting versatile electronic and magnetic properties.

2 Computational details

Our calculations were performed within the framework of density functional theory (DFT),[24] as implemented in the QUANTUM ESPRESSO code.[25] The exchange correlation energy was in the form of the Perdew–Burke–Ernzerhof (PBE) functional[26] with the generalized gradient approximation (GGA). The Brillouin zones were sampled with $12 \times 1 \times 1$ and $20 \times 1 \times 1$ Monkhorst–Pack k meshes for the armchair and zigzag NRs, respectively. The cutoff energy for the plane-wave expansion was set to 40 Ry. Both the k meshes and cutoff energy were carefully tested so that the electronic structures were converged. The distance between each NR and its periodic image was set to be larger than 10 Å so that they can be treated as independent entities.

3 Results and discussion

The ZrS_2 NRs can be obtained by cutting the monolayer. There are mainly two kinds of ZrS_2 NR, *i.e.* armchair and zigzag NRs, according to the cutting directions with respect to the monolayer. For the zigzag ZrS_2 NRs, the edges can be terminated by Zr or S atoms, thus three cases exist. We denote the case in which the two edges are both S atom-terminated as a 1S–1S zigzag NR, and the other two cases are 1Zr–1S (where one edge is a Zr atom and the other edge is an S atom) and 1Zr–1Zr (where both edges are Zr atoms) zigzag NRs. The relaxed structures of the four kinds of ZrS_2 NR are demonstrated in Fig. 1, where the left and right panels show top and side views, respectively. The width of the NR is defined according to the number of Zr atoms across the ribbon width, as shown in Fig. 1(a) and (c). Compared with the initial structures, the fully relaxed structures of the NRs change slightly. This is mainly due to the edge atoms, as the edge S atoms tend to migrate away from the inner atoms, while the Zr atoms prefer to approach the inner side.

To investigate the stability of the ZrS_2 NRs, we calculated the binding energy, E_b, which is defined as $E_b = (E_{Zr_nS_m} - nE_{Zr} - mE_S)/(n+m)$, where $E_{Zr_nS_m}$, E_{Zr} and E_S are the total energies of the ZrS_2 NRs and the Zr and S atoms, respectively. The larger the binding energy, the more stable the corresponding structure. The NRs with the width $N = 4$–14 are considered in this work. The calculated binding energies of the four kinds of ZrS_2 NR are in the range of 6.19–6.66 eV per atom, indicating that all of the investigated NRs are very stable. Moreover, as shown in Fig. 2, the binding energies of the 1S–1S zigzag NRs are the highest among the four kinds of NR, indicating that this type of NR is the most stable, followed by the armchair NRs, and the 1S–1Zr and 1Zr–1Zr zigzag NRs are relatively less stable. For each kind of NR, the system becomes more and more stable as the ribbon width increases.

To check the possibility of magnetism in ZrS_2 NRs, both spin-unpolarized and spin-polarized calculations were carried out. For the 1S–1Zr and 1Zr–1Zr zigzag NRs, the total energies of the FM states are lower than those of the nonmagnetic states,

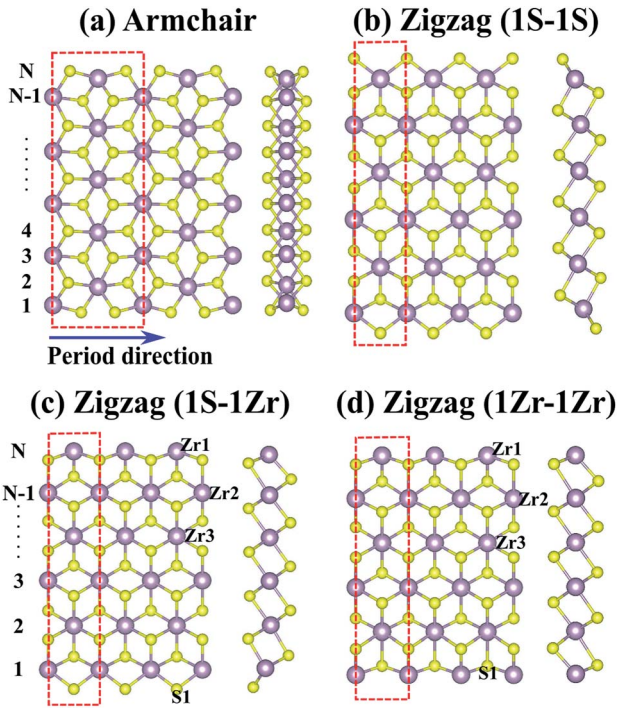

Fig. 1 Top and side views of the four different configurations of ZrS_2 NRs: (a) armchair, (b) 1S–1S zigzag, (c) 1S–1Zr zigzag and (d) 1Zr–1Zr zigzag NRs. The red dashed squares indicate the unit cell.

indicating that these two kinds of NR have a magnetic ground state. However, the other two cases, *i.e.* the armchair and 1S–1S zigzag NRs, are nonmagnetic. Firstly, we focus on the electronic properties of the nonmagnetic armchair and 1S–1S zigzag ZrS_2 NRs. The band structures show that all the investigated armchair ZrS_2 NRs are indirect band gap semiconductors (see Fig. 3(a)). The band gap exhibits interesting odd–even oscillation as the ribbon width increases (Fig. 3(d)), that is, the even-numbered NRs have relatively larger band gaps than the neighboring odd-numbered NRs. Moreover, the band gap of the

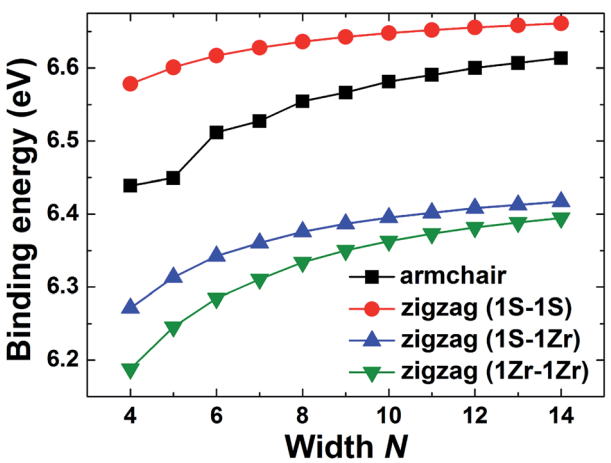

Fig. 2 Binding energies of the four kinds of ZrS_2 NR as a function of ribbon width.

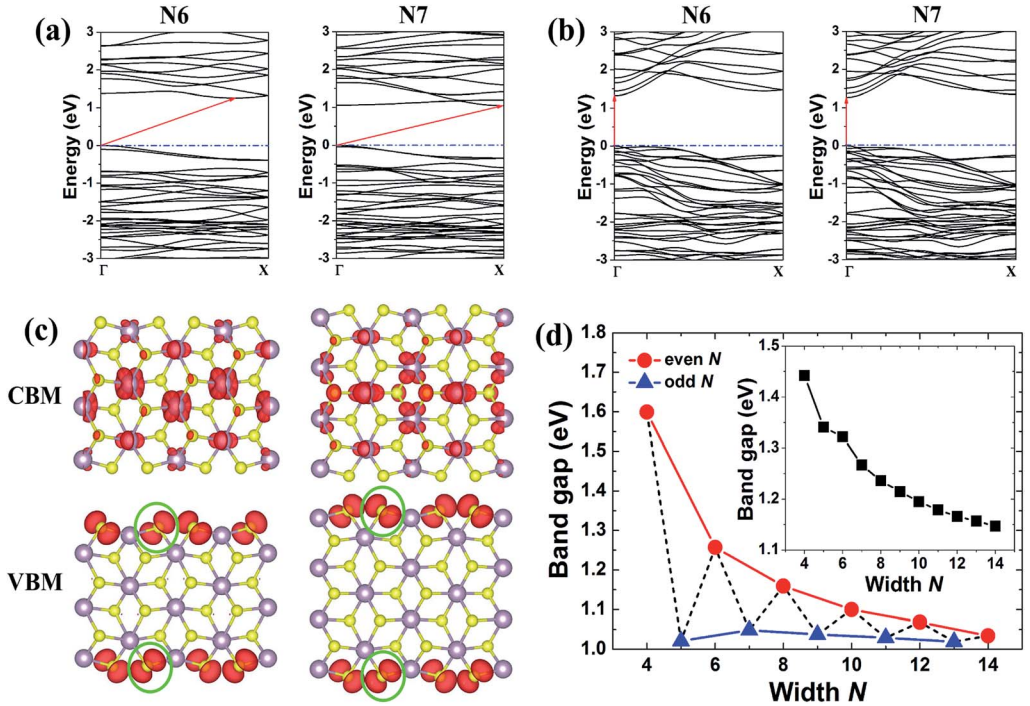

Fig. 3 Band structures of the two kinds of semiconducting ZrS_2 NRs: (a) armchair and (b) 1S–1S zigzag NRs with widths $N = 6$ and 7. (c) The band-decomposed charge densities for the conduction band minimum (CBM) and valence band maximum (VBM) of the armchair NRs with width $N = 6$ (left panel) and $N = 7$ (right panel). (d) Width-dependent band gap of the armchair ZrS_2 NRs. The inset is the result for the 1S–1S zigzag NRs.

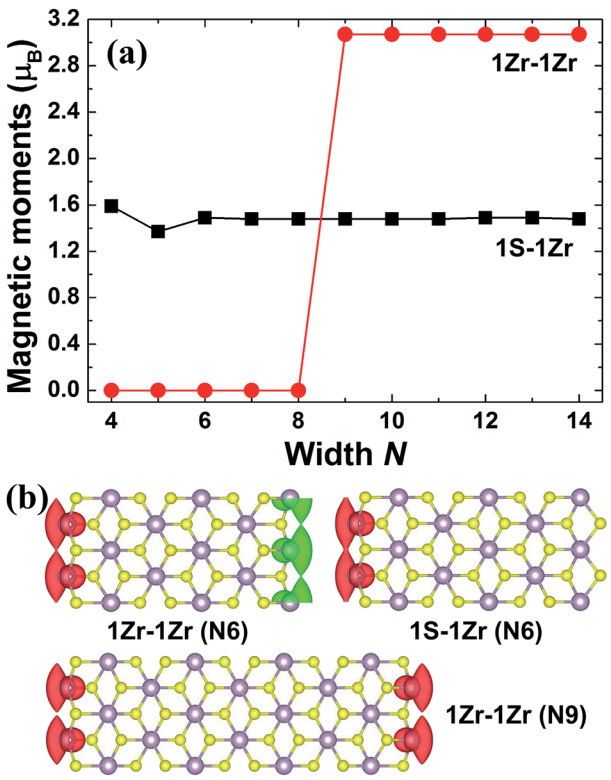

Fig. 4 (a) Total magnetic moments of the 1S–1Zr and 1Zr–1Zr zigzag ZrS_2 NRs. (b) Spin densities ($\rho\uparrow - \rho\downarrow$) for 1Zr–1Zr ($N = 6$), 1S–1Zr ($N = 6$) and 1Zr–1Zr ($N = 9$) NRs.

even-numbered NRs decreases as a function of the width, while it changes slightly for the odd-numbered NRs. On the other hand, all the 1S–1S zigzag NRs are semiconducting as well but have direct band gaps (Fig. 3(b)). The band gap decreases monotonically as the ribbon width increases (see the inset of Fig. 3(d)). Although the ZrS_2 monolayer is an indirect band gap semiconductor,[21] which makes it investigated less than MoS_2, the indirect-direct band gap transition can be obtained by cutting it into a 1D zigzag NR with both edges terminated by S atoms.

To investigate the origin of the odd–even oscillation of the band gap, we plot in Fig. 3(c) the band-decomposed charge densities for armchair ZrS_2 NRs with widths $N = 6$ and 7. We can see from Fig. 3(a) that for the armchair NRs, the valence band maximum (VBM) locates at the Γ point for both the even- and odd-numbered NRs, while the conduction band minimum (CBM) locates at the X points for the odd-numbered NRs and at the position between the Γ and X points for the even-numbered ones. The corresponding charge densities for the CBM and VBM are plotted in the upper and lower panels in Fig. 3(c), respectively. We can see that the CBM is mainly determined by the Zr atoms located in the inner part of the NRs, and there are much smaller contributions coming from the edge atoms. Therefore, the edge configurations have little impact on the electronic properties of the CBM. In contrast, the VBM is mainly controlled by the S atoms at the edge of the NRs. The structures of the odd-numbered NRs are symmetric with respect to the central line, thus the two nearest-neighboring S atoms at the two edges (which are circled by green lines) are just opposite

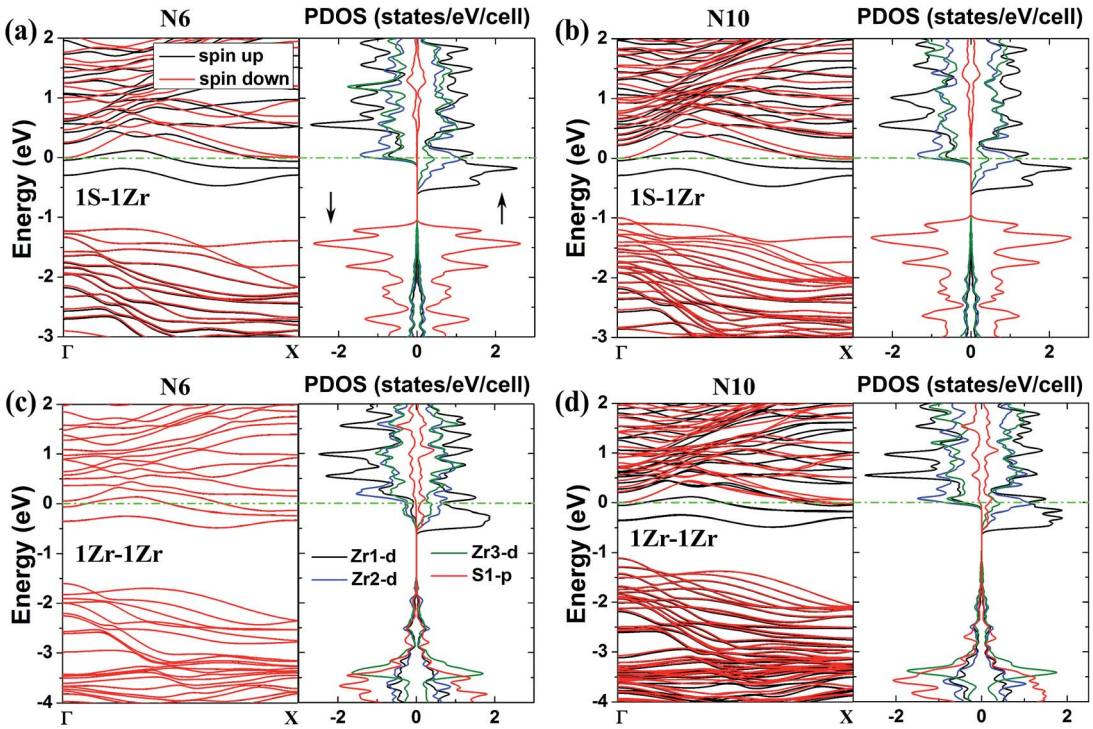

Fig. 5 Band structures and partial density of states (PDOS) of the two kinds of magnetic ZrS_2 NR: (a) 1S–1Zr ($N = 6$), (b) 1S–1Zr ($N = 10$), (c) 1Zr–1Zr ($N = 6$) and (d) 1Zr–1Zr ($N = 10$) NRs. The black and red lines denote the spin-up and spin-down states, respectively. For the PDOS, the results of four kinds of atom (denoted in Fig. 1(c) and (d)), the edge S atom (S1), edge Zr atom (Zr1) and two inner Zr atoms near the edge (Zr2 and Zr3), are shown.

each other, making their distance shortest for the two edge atoms. However, for the even-numbered NRs, the two nearest-neighboring S atoms at the two opposite edges are staggered. Their distance is therefore enlarged, making interactions between the two edges relatively smaller. As a result, the VBM is lowered for the even-numbered NRs and their band gaps are enlarged accordingly compared with those of the neighboring odd-numbered NRs.

As discussed above, the other two kinds of ZrS_2 NR, *i.e.* 1S–1Zr and 1Zr–1Zr zigzag NRs, are magnetic. The results of the spin density calculations (Fig. 4(b)) demonstrate that the magnetism of both systems mainly originates from the unsaturated edge Zr atoms. This is different from the H-structured zigzag MoS_2 NRs, whose magnetic moments are concentrated on both the edge Mo and S atoms.[8] For narrow graphene NRs, the spins of the two edges are antiparallel to each other, *i.e.* the two edges are antiferromagnetically coupled.[1] Since the 1Zr–1Zr ZrS_2 NRs have both edges terminated by Zr atoms, we also investigate the case in which the Zr atoms at the two edges are antiferromagnetically coupled. When the width $N = 4$–8, the energies of the AFM states are relatively smaller than those of the FM states, thus the ground states of the NRs are AFM. When the width increases up to 9, the system tends to be FM. A similar property was also observed in zigzag graphene NRs, for which switching from AFM to FM states may occur when the ribbon width is larger than 7 nm, due to FM inter-edge coupling.[27,28] For both the 1S–1Zr and 1Zr–1Zr zigzag NRs, the magnetic moments for the FM states are nearly width-independent, as shown in Fig. 4(a). Since both edges of the 1Zr–1Zr NR are terminated by Zr atoms, while for the 1S–1Zr NR there is only one edge of Zr atoms, the total magnetic moments of the 1Zr–1Zr NRs are twice those of the 1S–1Zr systems.

In Fig. 5, we plot the band structures and partial density of states (PDOS) for the 1S–1Zr and 1Zr–1Zr zigzag NRs with ribbon widths $N = 6$ and 10. The spin-up and spin-down channels are drawn in black and red lines, respectively. For the PDOS, the results of four kinds of atoms (denoted in Fig. 1(c) and (d)), including the edge S atom (S1), edge Zr atom (Zr1) and two inner Zr atoms near the edge (Zr2 and Zr3), are shown. For the 1S–1Zr ZrS_2 NRs (Fig. 5(a) and (b)), the spin-up channels are metallic while the spin-down channels are semiconducting, thus the NRs are 100% spin-polarized and the systems are FM half-metals. The results of the PDOS show that for S1, the spin-up and spin-down channels are symmetric, so it has no contribution to the magnetic moment. For Zr1, Zr2 and Zr3, the spin-up and spin-down channels are asymmetric. The edge Zr atom (Zr1) contributes most to the magnetic moment, and from the edge to the inner sites, the contribution becomes smaller and smaller. Therefore, the magnetic moments mainly originate from the unsaturated Zr atoms located at the edge, which is consistent with the results of the spin density calculations (Fig. 4(b)). For the 1Zr–1Zr ZrS_2 NRs, both the spin-up and spin-down states are metallic when $N \leq 8$ (Fig. 5(c)), thus the systems are AFM metals. However, the system tends to be a FM half-metal when N increases up to 9 and the magnetic moments mainly come from the Zr atoms at the two edges.

Compared with the H-structured MoS_2 NRs, the T-structured MX_2 NRs have been investigated less. Reyes-Retana *et al.* reported that zigzag $NiSe_2$ NRs are metallic and the armchair systems are semiconducting, but both of these are nonmagnetic.[29] Our results demonstrate that for the 1S–1Zr and 1Zr–1Zr zigzag ZrS_2 NRs, 1D electrical current with complete spin polarization can be realized along the Zr edges of the systems. The intrinsic half-metallicity predicted in the ZrS_2 NRs is highly desirable for applications in spintronics.

4 Conclusion

In conclusion, we have investigated the electronic and magnetic properties of ZrS_2 NRs. Armchair ZrS_2 NRs are indirect band gap semiconductors and the gap exhibits odd–even oscillation as the ribbon width increases. For zigzag ZrS_2 NRs, the 1S–1S NRs are direct band gap semiconductors and the gap decreases as the width increases. Both the armchair and 1S–1S zigzag ZrS_2 NRs are nonmagnetic. However, the 1S–1Zr and 1Zr–1Zr ($N \geq 9$) zigzag NRs are found to be FM half-metals and the magnetism mainly comes from the edge Zr atoms. Our results indicate that by tuning the edge configurations, ZrS_2 NRs could exhibit rich electronic and magnetic properties. The properties of direct gap and half-metallic ferromagnetism make ZrS_2 NRs promising candidates for future applications in electronics and spintronics.

Acknowledgements

This work was supported by the National Key Research and Development Program under Contract No. 2016YFA0300404, National Natural Science Foundation of China under Contract No. 11404340, 11674326 and U1232139, the Key Research Program of Frontier Sciences of CAS (QYZDB-SSW-SLH015), Hefei Science Center of CAS (2016HSC-IU011), and the Anhui Provincial Natural Science Foundation under Contract No. 1708085QA18. The calculation was partially performed at the Center for Computational Science, CASHIPS.

References

1 Y.-W. Son, M. L. Cohen and S. G. Louie, *Phys. Rev. Lett.*, 2006, **97**, 216803.
2 X. Li, X. Wang, L. Zhang, S. Lee and H. Dai, *Science*, 2008, **319**, 1229–1232.
3 Y.-W. Son, M. L. Cohen and S. G. Louie, *Nature*, 2006, **444**, 347–349.
4 O. Hod, V. Barone, J. E. Peralta and G. E. Scuseria, *Nano Lett.*, 2007, **7**, 2295–2299.
5 E.-j. Kan, Z. Y. Li, J. L. Yang and J. G. Hou, *J. Am. Chem. Soc.*, 2008, **130**, 4224–4225.
6 K. F. Mak, C. Lee, J. Hone, J. Shan and T. F. Heinz, *Phys. Rev. Lett.*, 2010, **105**, 136805.
7 A. Kuc, N. Zibouche and T. Heine, *Phys. Rev. B: Condens. Matter Mater. Phys.*, 2011, **83**, 245213.
8 Y. Li, Z. Zhou, S. Zhang and Z. Chen, *J. Am. Chem. Soc.*, 2008, **130**, 16739–16744.
9 A. R. Botello-Méndez, F. López-Urías, M. Terrones and H. Terrones, *Nanotechnology*, 2009, **20**, 325703.
10 H. Zhang, X.-B. Li and L.-M. Liu, *J. Appl. Phys.*, 2013, **114**, 093710.
11 S. Tongay, S. S. Varnoosfaderani, B. R. Appleton, J. Wu and A. F. Hebard, *Appl. Phys. Lett.*, 2012, **101**, 123105.
12 D. Gao, M. Si, J. Li, J. Zhang, Z. Zhang, Z. Yang and D. Xue, *Nanoscale Res. Lett.*, 2013, **8**, 129.
13 R. Zhang, Y. Li, J. Qi and D. Gao, *Nanoscale Res. Lett.*, 2014, **9**, 586.
14 Z. Yang, D. Gao, J. Zhang, Q. Xu, S. Shi, K. Tao and D. Xue, *Nanoscale*, 2015, **7**, 650–658.
15 N. Huo, Y. Li, J. Kang, R. Li, Q. Xia and J. Li, *Appl. Phys. Lett.*, 2014, **104**, 202406.
16 L. Zhang, L. Wan, Y. Yu, B. Wang, F. Xu, Y. Wei and Y. Zhao, *J. Phys. Chem. C*, 2015, **119**, 22164–22171.
17 H. Pan and Y.-W. Zhang, *J. Phys. Chem. C*, 2012, **116**, 11752–11757.
18 L. Kou, C. Tang, Y. Zhang, T. Heine, C. Chen and T. Frauenheim, *J. Phys. Chem. Lett.*, 2012, **3**, 2934–2941.
19 K. Dolui, C. D. Pemmaraju and S. Sanvito, *ACS Nano*, 2012, **6**, 4823–4834.
20 T. Hu, J. Zhou, J. Dong and Y. Kawazoe, *J. Appl. Phys.*, 2014, **116**, 064301.
21 Y. Li, J. Kang and J. Li, *RSC Adv.*, 2014, **4**, 7396–7401.
22 Y.-L. Zhang, X.-C. Wu, Y.-R. Tao, C.-J. Mao and J.-J. Zhu, *Chem. Commun.*, 2008, **2683**, 2683–2685.
23 L. Li, X. Fang, T. Zhai, M. Liao, U. K. Gautam, X. Wu, Y. Koide, Y. Bando and D. Golberg, *Adv. Mater.*, 2010, **22**, 4151–4156.
24 P. Hohenberg and W. Kohn, *Phys. Rev.*, 1964, **136**, B864.
25 P. Giannozzi, S. Baroni, N. Bonini, M. Calandra, R. Car, C. Cavazzoni, D. Ceresoli, G. L. Chiarotti, M. Cococcioni, I. Dabo, A. Dal Corso, S. de Gironcoli, S. Fabris, G. Fratesi, R. Gebauer, U. Gerstmann, C. Gougoussis, A. Kokalj, M. Lazzeri, L. Martin-Samos, N. Marzari, F. Mauri, R. Mazzarello, S. Paolini, A. Pasquarello, L. Paulatto, C. Sbraccia, S. Scandolo, G. Sclauzero, A. P. Seitsonen, A. Smogunov, P. Umari and R. M. Wentzcovitch, *J. Phys.: Condens. Matter*, 2009, **21**, 395502.
26 J. P. Perdew, K. Burke and M. Ernzerhof, *Phys. Rev. Lett.*, 1996, **77**, 3865.
27 G. Z. Magda, X. Jin, I. Hagymási, P. Vancsó, Z. Osváth, P. Nemes-Incze, C. Hwang, L. P. Biró and L. Tapasztó, *Nature*, 2014, **514**, 608–611.
28 J. Jung and A. H. MacDonald, *Phys. Rev. B: Condens. Matter Mater. Phys.*, 2009, **79**, 235433.
29 J. A. Reyes-Retana, G. G. Naumis and F. Cervantes-Sodi, *J. Phys. Chem. C*, 2014, **118**, 3295–3304.

